Pure Appl. Chem., Vol. 80, No. 11, pp. 2543–2552, 2008.
doi:10.1351/pac200880112543

B-site substituted lanthanum strontium ferrites as electrode materials for electrochemical applications*

Ulrich F. Vogt[1,4,‡], Josef Sfeir[3], Joerg Richter[2], Christian Soltmann[2], and Peter Holtappels[2]

[1]Laboratory of Hydrogen and Energy, EMPA, Swiss Federal Laboratories for Materials Testing and Research, Ueberlandstr. 129, 8600 Duebendorf, Switzerland; [2]Laboratory of High Performance Ceramics, EMPA, Swiss Federal Laboratories for Materials Testing and Research, Ueberlandstr. 129, 8600 Duebendorf , Switzerland; [3]Hexis Ltd., CH 8404, Winterthur, Switzerland; [4]Department of Crystallography, University of Freiburg, D-79104 Freiburg, Germany

Abstract: For electrochemical systems such as solid oxide fuel cells (SOFCs) or solid oxide electrolyzer cells (SOECs), perovskites are widely used as cathode material for the reduction of molecular oxygen. At present, strontium-substituted lanthanum manganite, $La_{1-x}Sr_xMnO_{3-\delta}$ (LSM), is used as standard SOFC cathode material for operation at high temperatures, whereas strontium-substituted lanthanum ferrite (LSF) is alternatively explored for medium-temperature SOFCs. Moreover, LSF is considered to be a potential candidate for oxygen separation membranes as the material reported interesting electrical properties. The design of new perovskite-type La transition-metal oxides is of significant technological importance in order to reduce the operating temperature to 600–800 °C and thus to reduce the SOFC system cost.

For investigations on a new material class, $(La_{1-x}Sr_x)_yFe_{1-z}(Ni,Cu)_zO_{3-\delta}$ was synthesized by a spray-pyrolysis process and modified on the A-site in both stoichiometric and non-stoichiometric configurations and on the B-site by substituting Fe with Ni and Cu.

Keywords: perovskites; synthesis; single-phase materials; CTE; electrochemistry.

INTRODUCTION

Perovskite-type materials are widely applied for high-temperature electrochemical devices such as solid oxide fuel cells (SOFCs), solid oxide electrolyzer cells (SOECs), and oxygen separation membranes. The crystal structure of perovskite-type materials can tolerate extensive modifications regarding its composition and shows promising physical and chemical features. The A- and/or B-site cations can partly be replaced in order to improve physical and chemical properties such as electrical conductivity, catalytic activity, electrode–electrolyte compatibility, or thermal and mechanical stability, which can play an important role for diverse applications. Although the basic strategies for improving certain properties are understood, detailed investigations to reveal dependencies of physical and chemical properties on the chemical composition are still required.

*Paper based on a presentation at the 3rd International Symposium on Novel Materials and Their Synthesis (NMS-III) and the 17th International Symposium on Fine Chemistry and Functional Polymers (FCFP-XVII), 17–21 October 2007, Shanghai, China. Other presentations are published in this issue, pp. 2231–2563.

‡Corresponding author

Strontium-substituted lanthanum manganite, $La_{1-x}Sr_xMnO_{3-\delta}$ (LSM), for example, is the state-of-the-art cathode material for the reduction of molecular oxygen in high-temperature SOFC applications. Lanthanum strontium ferrite $(La_{1-x}Sr_x)_yFeO_{3-\delta}$ (LSF) is becoming increasingly important due to its unique properties such as higher electronic conductivity and better oxygen transport properties compared to LSM. A- and B-sites substituted LSF are promising candidates for electrode applications in SOFCs and SOECs, as materials for catalysts as well as for oxygen separation membranes and sensors [1–6].

In the LSF crystal structure, cation substitutions are expected to be widely accommodated on the La site (A-site) as well as on the Fe site (B-site), resulting in modifications in the catalytic and electronic properties. LSFs with different levels of Sr substitution and co-substituted on the B-site with Ni or Cu were synthesized by a modified spray-pyrolysis process [7–9] developed in-house, enabling the production up to 3 kg batches per day of the desired composition. In this paper, the materials properties have been studied regarding phase purity and composition, sintering behavior, and compatibility with yttria-stabilized zirconia (YSZ). The determination of the electronic properties and the linear coefficient of thermal expansion (CTE) has also been a focus of inquiry. This information is needed to evaluate the applicability of LSF as an electrode in solid oxide electrochemical cells, such as SOFCs and SOECs.

EXPERIMENTAL

A spray-pyrolysis device with a capacity of up to 3 kg powders per day was established for powder synthesis [11]. The set-up consists of an electrically heated furnace with a stainless-steel vessel equipped with a spraying nozzle in the center of the top cover. For the spray-pyrolysis process, water-based (deionized) high concentrated solutions of the requested compositions were prepared from solvated nitrates of $La(NO_3)_3{\cdot}6H_2O$ (Auer Remy, D, purity 99.98 %), $Sr(NO_3)_2$ (Riedel-de Haen, D, purity 98 %), $Fe(NO_3)_3{\cdot}9H_2O$ (Fluka, CH, purity 98 %) and $Ni(NO_3)_3{\cdot}6H_2O$ (Fluka, CH, purity 98 %), or $Cu(NO_3)_3{\cdot}3H_2O$ (Riedel-de Haen, D, purity 99 %), respectively. An adequate amount of gelatine (50 g/l) (Gewürzmüller, Germany) or citric acid (Fluka, Switzerland), was added to boost the reaction. The mixtures were homogenized on a magnetic stirrer at ~80 °C for about 40 min. The precursor solution of the respective nitrates was sprayed into the hot furnace (25 ml/min) along with air (330 ml/min, air pressure 3 bar) for atomization of the solution. The furnace temperature was varied from 300 to 700 °C for investigating the reaction conditions. The selected chemical compositions synthesized by spray-pyrolysis from nitrate-salt solutions are shown in Tables 1a and 1b. The synthesized powders were characterized by means of X-ray powder diffraction (XPD) (Cu–K_α, PANalytical X'Pert PRO MPD). The particle size distribution (PSD) was measured by laser diffraction analysis (Coulter LS 230), the specific surface area determined by gas adsorption according to the Brunauer–Emmett–Teller (BET) method (Coulter SA 3100) in combination with an out-gassing station (Coulter SA Prep).

Table 1a A-site variation for stoichiometric/nonstoichiometric compositions $(La_{1-x}Sr_x)_yFeO_{3-\delta}$.

P5	$(La_{0.8}Sr_{0.2})FeO_{3-\delta}$	P11	$(La_{0.7}Sr_{0.3})FeO_{3-\delta}$
P6	$(La_{0.8}Sr_{0.2})_{0.95}FeO_{3-\delta}$	P12	$(La_{0.6}Sr_{0.4})FeO_{3-\delta}$
P7	$(La_{0.8}Sr_{0.2})_{0.9}FeO_{3-\delta}$	P13	$(La_{0.8}Sr_{0.2})_{0.8}FeO_{3-\delta}$
P8	$(La_{0.8}Sr_{0.2})_{1.05}FeO_{3-\delta}$	P14	$(La_{0.7}Sr_{0.2})FeO_{3-\delta}$
P9	$(La_{0.8}Sr_{0.2})_{1.1}FeO_{3-\delta}$	P15	$(La_{0.6}Sr_{0.2})FeO_{3-\delta}$

Table 1b B-site variation for the compositions $(La_{1-x}Sr_x)_yFe_{1-z}(Ni, Cu)_zO_{3-\delta}$.

Z6	$(La_{0.8}Sr_{0.2})_{0.95}Ni_{0.2}Fe_{0.8}O_{3-\delta}$	Z10	$(La_{0.8}Sr_{0.2})_{0.95}Cu_{0.2}Fe_{0.8}O_{3-\delta}$
Z7	$(La_{0.8}\ Sr_{0.2})_{0.95}Ni_{0.4}Fe_{0.6}O_{3-\delta}$	Z11	$(La_{0.8}Sr_{0.2})_{0.95}Cu_{0.4}Fe_{0.6}O_{3-\delta}$
Z8	$(La_{0.8}Sr_{0.2})_{0.95}Ni_{0.6}Fe_{0.4}O_{3-\delta}$	Z12	$(La_{0.8}Sr_{0.2})_{0.95}Cu_{0.6}Fe_{0.4}O_{3-\delta}$
Z9	$(La_{0.8}Sr_{0.2})_{0.95}Ni_{0.8}Fe_{0.2}O_{3-\delta}$	Z13	$(La_{0.8}Sr_{0.2})_{0.9}{}^5Cu_{0.8}Fe_{0.2}O_{3-\delta}$

The as-synthesized powder was dry-milled with Zr balls of 10 mm diameter and subsequently annealed at temperatures from 900 to 1200 °C for studying the phase formation as a function of stoichiometry and annealing temperature. The final annealing temperature was selected by virtue of single-phase behavior of the various A-site and B-site stoichiometries. After temperature annealing, the powders were ground to the desired particle size $D_{50} < 1$ μm by wet-ball milling in deionized water with Zr balls of 2 mm diameter.

For determining the optimal sintering temperature, a sintering furnace (Ceram–Aix, Nabertherm) and sinter dilatometer (Baehr-Thermoanalysis, 802S, equipped with Al_2O_3 rods) were used. Sintering experiments were carried out on tablets of 13 mm diameter, pressed in an uniaxial press at 130 MPa. For the dilatometer measurements, bar-shaped samples of 3×4 mm and 10–15 mm in length were used. The heating rate for dilatometer experiments was 5 K/min up to sintering temperature and a holding time of 1 h. The sample was subsequently cooled down at a rate of 5 K/min.

The density of the sintered samples was determined by the Archimedes principle in water. Sintered samples of the size 5×55 mm were utilized for measurements of the CTE in air, using a dilatometer 802 S (Baehr Thermoanalyse GmbH, Germany) equipped with fused silica push rods. The change in length was recorded while the temperature was constantly increased by 5 K/min from room temperature to 1000 °C and cooled down with 5 K/min.

For material compatibility tests, 1:1 mixtures of the various LSF compositions with 8YSZ powder were pressed to tablets of 13 mm diameter and annealed at 1100 °C for 4 h and 800 °C for 300 h, which corresponds to the potential sintering, respectively working conditions for SOFC cathodes.

The electrical conductivity was determined as a function of temperature in a 4-point configuration, using either a Milli-Ohmmeter RESISTOMAT 2318 (Burster Praezisionsmesstechnik GmbH & Co. KG, Germany) or a Keithley Multimeter Model 2750/E (Keithley Instruments, USA). Bar-shaped samples with a length of 25–35 mm and a cross-section of 3×4 mm were contacted using Pt-wires spring-loaded on the samples allowing that the voltage drop was measured over a fixed distance. To enhance the contacting quality, strips where painted below the contacts using Pt-paste (CL11-5100, W. C. Heraeus GmbH & Co. KG, Germany).

RESULTS AND DISCUSSION

Powder synthesis and characterization

Various synthesis parameters like furnace temperature for spray pyrolysis (300, 400, 500, 600, and 700 °C), addition of gelatine or citric acid for boosting the reaction, and calcination temperature of the as-pyrolyzed powders were investigated. Principal process optimization has been carried out on the stoichiometric composition $(La_{0.8}Sr_{0.2})FeO_{3-\delta}$ (P5), and thus the synthesized powders characterized in relation to PSD, specific surface area (BET), and phase composition (XRD) [7]. From this analysis, it was observed that the influence of the spraying temperature was negligible concerning surface area and PSD after calcination above 1100 °C and a subsequent milling step. Thus, 500 °C has been established as standard temperature for the spray-pyrolysis process, as it was found to be the ideal temperature for the stability of the process. As additional fuel for boosting the reaction, gelatine was selected due to the lower price and distinctly lower required precursor concentration when compared to citric acid.

For the stoichiometric composition $(La_{0.8}Sr_{0.2})FeO_{3-\delta}$ (P5), a single-phase perovskite was obtained after calcination at 1200 °C (Fig. 1) showing orthorhombic symmetry (Pbnm) in agreement with the literature [12,13]. At lower calcination temperatures, the secondary phases of $LaFeO_3$ and $SrLaFeO_4$ were detected as previously described in literature [10]. The under-stoichiometric compositions $(La_{0.8}Sr_{0.2})_{0.95}FeO_{3-\delta}$ (P6) and $(La_{0.8}Sr_{0.2})_{0.9}FeO_{3-\delta}$ (P7) were also single-phase perovskites after annealing at 1200 °C. In contrast the overstoichiometric compositions of $(La_{0.8}Sr_{0.2})_{1.1}FeO_{3-\delta}$ (P8) and $(La_{0.8}Sr_{0.2})_{1.05}FeO_{3-\delta}$ (P9) show secondary phases of $SrLaFeO_4$ and $La_2SrFe_2O_7$ (Fig. 1).

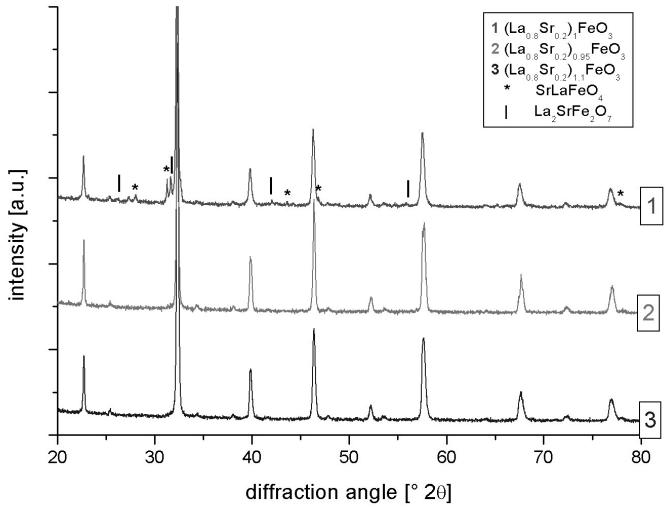

Fig. 1 XPDs of LSF with different A-site stoichiometries. 1: $(La_{0.8}Sr_{0.2})FeO_{3-\delta}$, (P5) 2: $(La_{0.8}Sr_{0.2})_{0.95}FeO_{3-\delta}$, (P6) 3: $(La_{0.8}Sr_{0.2})_{1.1}FeO_{3-\delta}$ (P9) with secondary phases of $SrLaFeO_4$ and $La_2SrFe_2O_7$.

Ni and Cu substitution for $(La_{0.8}Sr_{0.2})_{0.95}Fe_{1-z}(Ni,Cu)_zO_{3-\delta}$ (z = 0.2, 0.4, 0.6, 0.8) was investigated. It was observed that Ni substitution up to 20 mol % leads to single-phase materials (Z6). By replacing more than 20 mol % of Fe by Ni (Z7–Z9), secondary phases of NiO and $La_{2-x}Sr_xNiO_4$ where precipitated. The amount of secondary phases increased with higher Ni contents as shown in Fig. 2.

Cu-substituted perovskites (Z10–Z13) show a similar behavior. By replacing up to 20 mol % Fe by Cu, single-phase perovskites could be synthesized. At nominal Cu concentrations higher than 20 mol %, secondary phases such as $(La_{8-x}Sr_x)Cu_6Fe_2O_{20}$ were analyzed by XRD, the concentration of secondary phases rising with increasing Cu content.

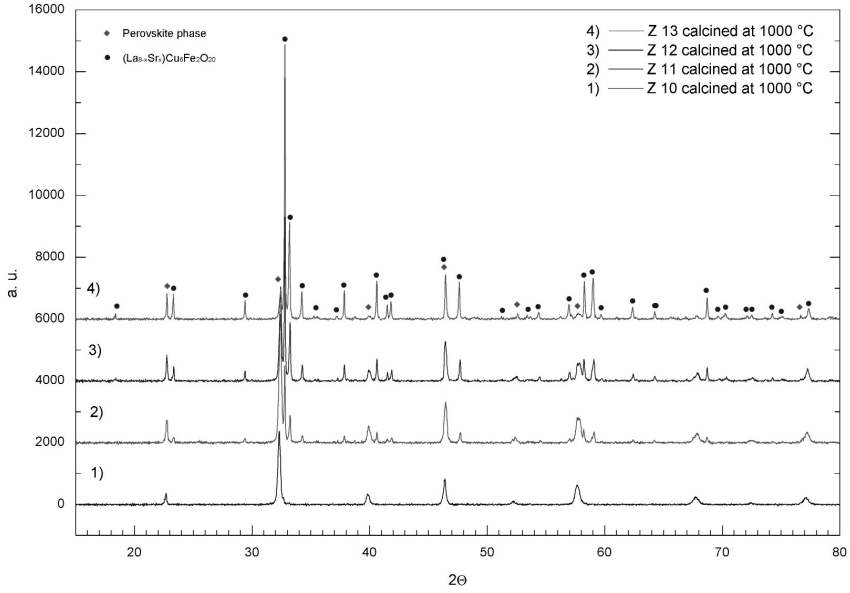

Fig. 2 XPDs of Ni-substituted LSF calcined at 1000 °C for 4 h. Observed secondary phases: NiO and $La_{2-x}Sr_xNiO_4$.

Sintering behavior and CTE

The influence of the chemical composition on the sintering and thus densification behavior was examined on perovskite powders which were calcined at 1200 °C. While the understoichiometric compositions $(La_{0.8}Sr_{0.2})_{0.95}FeO_{3-\delta}$ (P6) and $(La_{0.8}Sr_{0.2})_{0.9}FeO_{3-\delta}$ (P7) show a high shrinkage rate at 1400 °C, the overstoichiometric compositions $(La_{0.8}Sr_{0.2})_{1.05}FeO_{3-\delta}$ (P8) and $(La_{0.8}Sr_{0.2})_{1.1}FeO_{3-\delta}$ (P9) show only a small shrinkage rate. The shrinkage is related to the sintering behavior of the powders, which depends on the melting point. Thus, a higher melting point is observed for the overstoichiometric compositions. The stoichiometric compositions $(La_{0.7}Sr_{0.3})FeO_{3-\delta}$ (P11) and $(La_{0.6}Sr_{0.4})FeO_{3-\delta}$ (P12) proved to be close to the theoretical density when sintered at 1400 °C for 4 h. Similarly, the density of the under-stoichiometric compositions P13, P14, and P15 are above 90 % after sintering at 1300 °C for 4 h, but the density decreased when sintered higher than 1300 °C, according to the lower melting point. For compositions with 20 % Ni substitution on B-site (Z6, Fig. 3), a density of 95 % could be achieved at 1400 °C sintering temperature, whereas the composition with 20 % Cu substitution (Z10) could be sintered at only 1100 °C to a density of 92 % as at higher temperatures the melting point was reached (Table 2) [14].

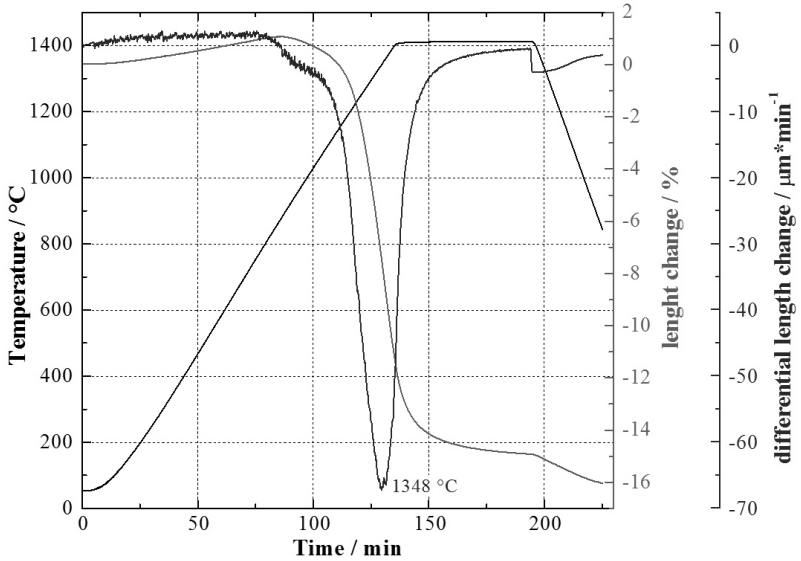

Fig. 3 Dilatometer sintergraph for the composition $(La_{0.8}Sr_{0.2})_{0.95}Ni_{0.2}Fe_{0.8}O_{3-\delta}$ (Z6) from 20 to 1400 °C.

Table 2 Influence of sintering conditions on the densification of LSF compositions.

Composition	1100 °C, 4 h	1200 °C, 4 h	1300 °C, 4 h	1400 °C, 4 h	1400 °C, 12 h
P11[b]	–	68 %[a]	–	94 %	96 %
P12[b]	–	68 %[a]	–	96 %	96 %
P13[b]	–	68 %[a]	90 %	69 %	–
P14[b]	–	61 %[a]	94 %	58 %	–
P15[b]	–	60 %[a]	92 %	74 %	–
Z6[b]	–	66 %[a]	–	95 %	94 %
Z10[c]	92 %	–	–	–	–

[a]Geometrical density.
–: not available
[b]Calcined at 1200 °C.
[c]Calcined at 900 °C.

Table 3 displays the coefficients of linear thermal expansion CTE (calculated and experimental) for several stoichiometric and non-stoichiometric compositions in the temperature range from 20 to 1000 °C. Note that the term "thermal expansion" is used here in a general way, since expansion may result not only from the prime thermal effect, but also as a secondary effect due to release or incorporation of oxygen in order to maintain the thermodynamical balance [10]. The expansion is found to be linear, and the CTE was 11.6×10^{-6} K^{-1} for the compositions P5 (Fig. 4), P6, and P8, measured between room temperature and 1000 °C. Such a linear behavior was generally observed for materials with A-site deficiency and A-site excess if the Sr content is below $x = 0.2$.

Table 3 Overview of the CTE for various LSF compositions.

Sample Nr	Composition	Expansion (20–1000 °C) linear regression 10^{-6} K^{-1}	Expansion (20–1000 °C) experimental range 10^{-6} K^{-1}
P5	$(La_{0.8}Sr_{0.2})FeO_{3-\delta}$	10.8	10.0–11.8
P6	$(La_{0.8}Sr_{0.2})_{0.95}FeO_{3-\delta}$	11.6	10.0–12.3
P8	$(La_{0.8}Sr_{0.2})_{1.05}FeO_{3-\delta}$	11.1	10.5–13.0
P11	$(La_{0.7}Sr_{0.3})FeO_{3-\delta}$	11.0 (20–775 °C) 12.0 (775–1000 °C)	9.0–11.5 (20–775 °C) 11.5–13.0 (775–1000 °C)
P12	$(La_{0.6}Sr_{0.4})FeO_{3-\delta}$	11.8 (20–750 °C) 13.2 (750–1000 °C)	11.5–13 (20–775 °C) 13.0–15.0 (750–1000 °C)
P14	$(La_{0.7}Sr_{0.2})FeO_{3-\delta}$	10.0	8.5–10.5
P15	$(La_{0.6}Sr_{0.2})FeO_{3-\delta}$	12.1	8.0–13.7
Z6	$(La_{0.8}Sr_{0.2})_{0.95}Ni_{0.2}Fe_{0.8}O_{3-\delta}$	10.47	10.5–11
Z10	$(La_{0.8}Sr_{0.2})_{0.95}Cu_{0.2}Fe_{0.8}O_{3-\delta}$	10.65	9.8–11.5

In contrast to the linear thermal expansion (P5), an increasing Sr content (P11, P12, Fig. 4) leads to a chemical expansion and thus to an increase in the relative length change at elevated temperatures as a result of the reduction of Fe^{3+} to the larger Fe^{4+} ion, causing an increasing oxygen non-stoichiometry. Release of oxygen creates additional vacancies, which can enhance the ionic conductivity [15]. For Sr contents of 30 and 40 %, two distinct temperature regions could be identified, resulting in apparent low- and high-temperature CTE values. A correlation can be stated for the interrelation of

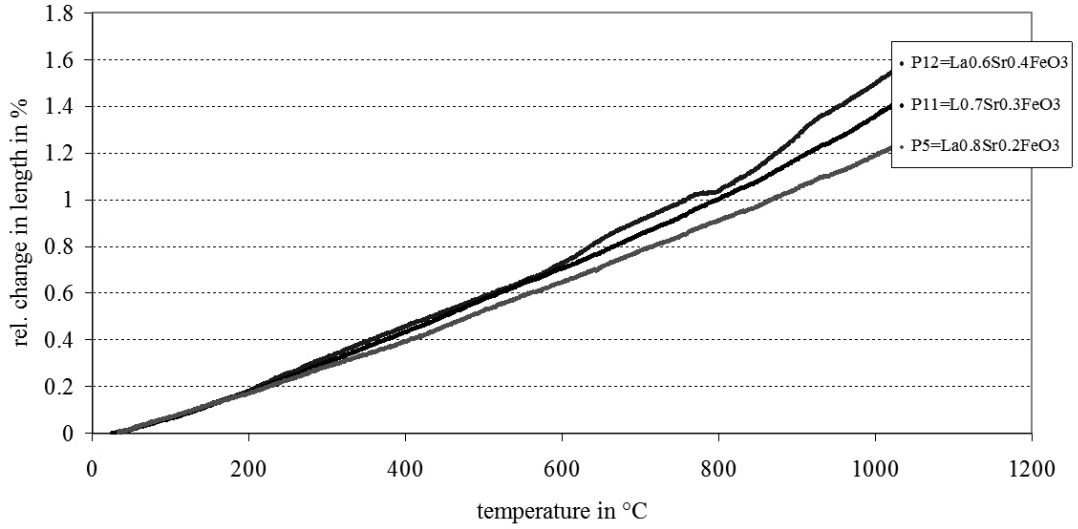

Fig. 4 Relative change in length [%] in relation to the Sr content in LSF.

stoichiometric A-site compositions (P5, P11, P12). The CTE value and the relative change in length increases slightly with raising Sr content (Fig. 4).

CTE measurements on Ni-substituted samples on B-site (Z6–Z9) show no significant influence on the relative length change, as they are all in the order of 1.35 to 1.45 % at 1000 °C. The calculated CTE values determined for the almost linear expansion curves are summarized in Fig. 5 for LSFs which are non-stoichiometric on the A-site. Large deviation from stoichiometry decreases the CTE considerably from values around 12×10^{-6} K^{-1} to $<8 \times 10^{-6}$ K^{-1}. Thus, slight understoichiometry on the A-site is favored to adjust the CTE of the perovskite to YSZ electrolytes [12]. The Ni- and Cu-substituted (Z6,

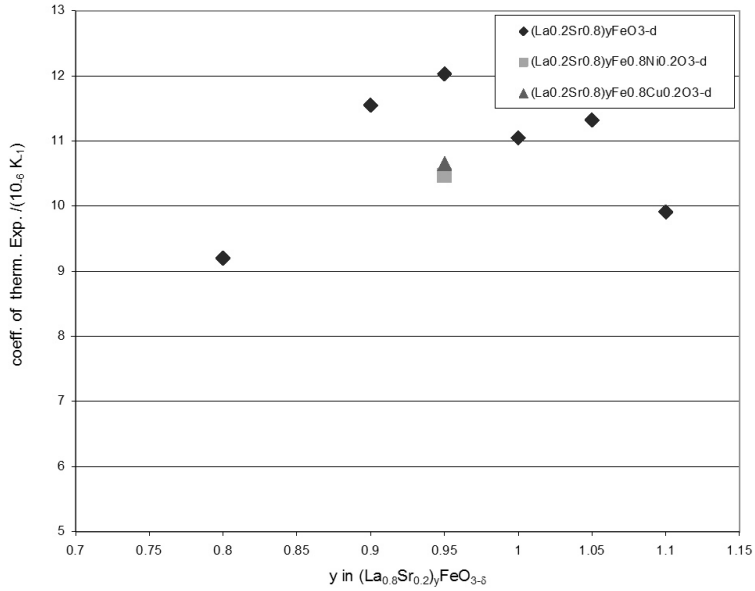

Fig. 5 CTE of LSF in dependence of A-site stoichiometry and B-site composition. The CTEs of Cu- and Ni-substituted perovskites are close to that of the 8 %YSZ electrolyte.

Z10) perovskites also match the thermal expansion coefficient of the standard 8YSZ electrolyte quite well.

Compatibility of LSF-8YSZ

Several LSF compositions and stoichiometries were investigated regarding reactions with 8YSZ, commonly used in SOFC systems. A mixture of LSF (P6) - 8YSZ, (50/50 vol %) was annealed at 800 °C for 300 h and at 1100 °C for 4 h. While at 800 °C/300 h, no material interactions could be detected by XRD, annealing at 1100 °C/4 h showed a small peak shift of the LSF at $2\Theta = 32.3°$, corresponding to a unit cell expansion due to incorporation of Zr and/or Y cations into the perovskite structure as reported by Simner and Fossad [10,12].

The under-stoichiometric compositions P 13, P14, and P15 show no secondary phases up to 1100 °C due to La^{3+} and Sr^{2+} deficiency. Moreover, no peak shift was discernible at 800 °C, respectively, 1000 °C. At 1100 °C, a small peak shift was observed, which may also correspond to a unit cell expansion. Stoichiometric mixtures of P11 and P12 with 8YSZ (50/50 vol %) show no reaction at 800 °C/300 h, however, for annealing temperatures of 1000 and 1100 °C/4 h, traces of $SrZrO_3$ as secondary phases could be located by XRD analysis.

Electrical conductivity

The conductivities as a function of temperature for LSFs with different stoichiometries of A- and B-site cations are shown in Fig. 6. While for low temperatures, a semi-conducting behavior is observed, the conductivity goes through a maximum at intermediate temperatures. This effect is most pronounced for 5 % excess of Fe on the B-site, but least for 10 % Fe deficiency. The conductivity at high temperatures, e.g., at 800 °C (Table 4), clearly decreases with increasing deviation from the stoichiometric A/B = 1 composition.

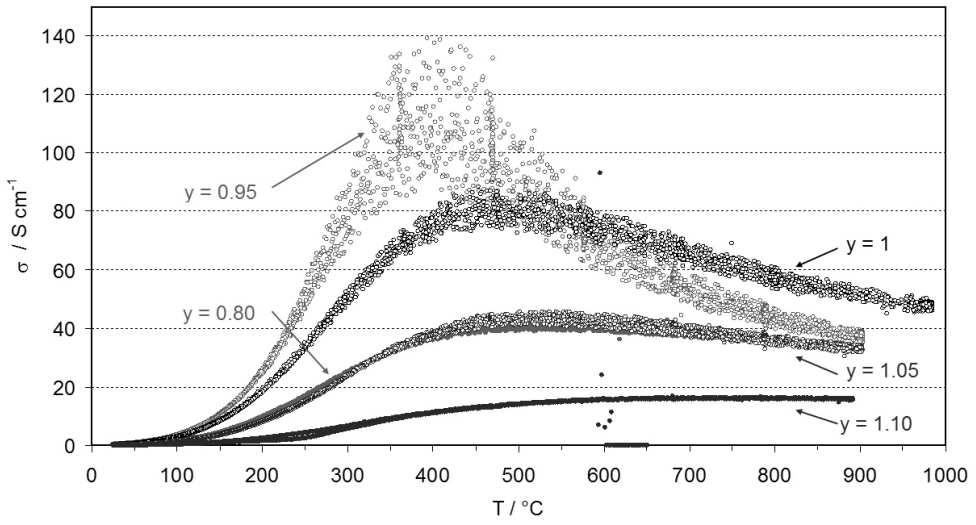

Fig. 6 Conductivity as a function of temperature for various LSFs with different stoichiometries of A- and B-site cations.

Table 4 Maximum conductivity σ_{max}, the related temperature and the conductivity at 800 °C, σ_{800}; relevant for the operation of a state-of-the-art SOFC.

Composition	σ_{max}/S cm^{-1}	T/°C	σ_{800}/S cm^{-1}
P5: $(La_{0.8}Sr_{0.2})FeO_{3-\delta}$	80	460	57
P6: $(La_{0.8}Sr_{0.2})_{0.95}FeO_{3-\delta}$	105	400	44
P13: $(La_{0.8}Sr_{0.2})_{0.8}FeO_{3-\delta}$	40	500	38
P8: $(La_{0.8}Sr_{0.2})_{1.05}FeO_{3-\delta}$	42	525	38
P9: $(La_{0.8}Sr_{0.2})_{1.10}FeO_{3-\delta}$	18	800	18
Z6: $(La_{0.8}Sr_{0.2})_{0.95}Fe_{0.8}Ni_{0.2}O_{3-\delta}$	420	410	175
Z10: $(La_{0.8}Sr_{0.2})_{0.95}Fe_{0.8}Cu_{0.2}O_{3-\delta}$	340	450	120

The decrease in conductivity is frequently observed for these materials and related to the loss of oxygen at elevated temperatures. Since these materials are predominant electronic hole conductors, increasing vacancy formation due to oxygen loss will depress the hole concentration and thus the overall conductivity according to defect chemistry equilibration.

It should be noted, that for the compositions with 5 % Fe excess, $(La_{0.8}Sr_{0.2})_{0.95}FeO_{3-\delta}$, $(La_{0.8}Sr_{0.2})_{0.95}Fe_{0.8}Ni_{0.2}O_{3-\delta}$, and $(La_{0.8}Sr_{0.2})_{0.95}Fe_{0.8}Cu_{0.2}O_{3-\delta}$, a significant scatter in the data around the maximum conductivity was observed. Since the scatter was not obvious for other samples in the same set-up for similar conductivities, this feature needs to be attributed to the materials rather than to the set-up. A tentative explanation is a change in the magnetic properties that make these compositions sensitive to AC perturbations from the furnace heating elements. The average values for the maximum conductivity σ_{max}, the related temperature, and the conductivity at 800 °C, σ_{800} relevant for the operation of a state-of-the-art SOFC are summarized in Table 4.

Both, Ni and Cu substitution increases the total conductivity. However, Ni substitution shows superior conductivities both, at the maximum conductivity and at 800 °C.

CONCLUSION

It could be shown that A- and B-site substituted LSF perovskites with varying stoichiometries can be produced by means of spray pyrolysis. The following nominal compositions were investigated: $(La_{1-x}Sr_x)_yFeO_{3-\delta}$, with x = 0.2, 0.3, 0.4; y = 0.8, 0.9, 0.95, 1, 1.05, 1.1; and $(La_{1-x}Sr_x)_yFe_{1-z}(Ni, Cu)_zO_{3-\delta}$, with x = 0.2, y = 1, 0.95, z = 0.2, 0.4, 0.6, 0.8. Phase purity was affected by the stoichiometry and the annealing temperature. The calcination temperature for single-phase powders has been evaluated for various perovskite compositions by means of XPD studies. The over-stoichiometric compositions indicate secondary phases, independent of the calcination temperature. Stoichiometric and under-stoichiometric compositions become single-phase perovskites after calcination at 1200 °C. It could also be demonstrated that the substitution of Fe by Ni or Cu on the B-site, $(La_{0.2}S_{0.8})_{0.95}Ni/Cu_xFe_{1-x}O_3$, is viable, but the substitution is limited to 20 mol % Ni or Cu. Cu substitution and under-stoichiometry lower the melting point and thus consequently the sintering temperature of the perovskites.

Non-stoichiometric LSF compositions showed a correlation between stoichiometry and apparent linear thermal expansion. For matching the CTE of LSF with YSZ, 15 % A-site deficiency is reflected to be favorable. The Ni-substituted LSF showed the highest conductivity in the series of compositions investigated in this study.

ACKNOWLEDGMENTS

This work was carried out with financial support from the European Commission under the 6th Framework Programme, in the Integrated Project Real-SOFC (contract no. SES6-CT-2003-502612).

The authors also would like to thank Adrian Fries and Lubomir Hric who did their diploma work on this topic, Maik Thünemann and H. J. Schindler for the dilatometer and CTE measurements, and Dr. Artur Braun for fruitful discussion of the conductivity.

REFERENCES

1. A. Leonidov, V. L. Kozhevnikov, M. V. Patrakeev, E. B. Mitberg, K. R. Poeppelmeier. *Solid State Ionics* **144**, 361 (2001).
2. S. Diethelm, J. Van herle, J. Sfeir, P. Buffat. *J. Eur. Ceram. Soc.* **25**, 2191 (2005).
3. P. J. Gellings, H. J. M. Bouwmeester. *Catal. Today* **58**, 1 (2000).
4. P. J. Gellings, H. J. M. Bouwmeester. *Catal. Today* **12**, 1 (1992).
5. J. Sfeir, P. Buffat, P. Mockli, N. Xanthopoulos, R. Vasquez, H. J. Mathieu, J. Van herle, K. R. Thampi. *J. Catal.* **202**, 229 (2001).
6. M. V. Patrakeev, I. A. Leonidov, V. L. Kozhevnikov, K. R. Poeppelmeier. *J. Solid State Chem.* **178**, 921 (2005).
7. J. Sfeir, S. Vaucher, P. Holtappels, U. Vogt, H.-J. Schindler, J. Van herle, E. Suvorova, P. Buffat, D. Perret, N. Xanthopoulos, O. Bucheli. *J. Eur. Ceram. Soc.* **25**, 1991 (2005).
8. P. Holtappels, U. F. Vogt, H.-J. Schindler, B. Gut. *Perovskite Synthesis by Spray Pyrolysis, 5th European Solid Oxide Fuel Cell Forum*, Vol. 1, J. Huijsmans (Ed.), pp. 103–107, Lucerne, Switzerland (2002).
9. G. L. Messing, S. C. Zhang, G. V. Jayanthi. *J. Am. Ceram. Soc*. **76**, 2702 (1993).
10. S. P. Simner, J. P. Shelton, M. D. Anderson, J. W. Stevenson. *Solid State Ionics* **161**, 11 (2003).
11. P. Holtappels, U. Vogt, T. Graule. *Adv. Eng Mater*. **7**, 292 (2005).
12. A. Fossad, M. Menon, I. Warnhus, K Wiik, A. A. Einarsrud, T. Grande. *J. Am. Ceram. Soc.* **87**, 1952 (2004).
13. M. Mogi, Y. Inoune, M. Arano, Y. Koyama. *Physica C* **392–396**, 295 (2003).
14. U. F. Vogt, J. Sfeir, C. Soltmann, P. Holtappels. *Proc. 7th European Solid Oxide Fuel Cell Forum*, Lucerne, P-0630, European Fuel Cell Forum, Oberrohrbach, Switzerland (2006).
15. M. V. Patrakeev, J. A. Bathteeva, E. B. Mitberg, I. A. Leonidov, V. L. Kozhevnikov, K. R. Poeppelmeier. *J. Solid State Chem.* **172**, 219 (2003).